

Geminga: A Window of the Role Played by Local Halo in the Cosmic Ray Propagation Process

LIN NIE,^{1,2,3} YU-HAI GE,³ YI-QING GUO,³ AND SI-MING LIU²

¹*School of Mechanics and Aerospace Engineering, Southwest Jiaotong University, Chengdu, 610031, China*

²*School of Physical Science and Technology, Southwest Jiaotong University, Chengdu, 610031, China*

³*Key Laboratory of Particle Astrophysics, Institute of High Energy Physics, Chinese Academy of Sciences, Beijing, 100049, China*

ABSTRACT

An emerging commonality among the recently observed pulsar halos is the presence of distinct radiation patterns at high energies, while no extended radiation is detected around the GeV energy band. This commonality suggests that pulsar halos play a crucial role in the local propagation of cosmic rays, making it necessary to investigate the underlying mechanisms of this phenomenon. This work focuses on the 3D propagation study of cosmic rays, incorporating the Geminga pulsar into our propagation model to investigate its contribution to different observational spectra. We consider Geminga a dominant local source of positrons, successfully reproducing the observed positron spectrum and multi-energy spectra of the Geminga halo. Through calculations of signal and background at different angles, we find that: (1) at low energies, the slow diffusion characteristic around the pulsar region leads to a low electron density in the extended area around Geminga, causing the background radiation to exceed the signal intensity far; (2) at high energies, the larger effective diffusion radius of high-energy electrons/positrons causes the signal from Geminga to dominate the local high-energy phenomena; (3) the observed fluctuation of diffuse gamma-ray radiation by LHAASO is likely due to the incomplete subtraction of radiation from the local halo. We hope LHAASO will detect more cosmic ray halo sources to validate our model further.

Keywords: Geminga, Cosmic ray propagation, Diffuse γ -ray emission

1. INTRODUCTION

As cosmic ray observation experiments enter an era of precision, traditional cosmic ray propagation models cannot predict some finer spectral structures. For instance, primary CR spectra exhibit a spectral hardening at high energies. Data from AMS-02 reveals that the CR spectra above several hundred GeV deviate from a simple power law, displaying a spectral hardening, a phenomenon now confirmed across various experimental platforms (Aguilar et al. 2021; An et al. 2019; Atkin et al. 2018). Secondary CR spectra also harden at this energy range, and their spectra are steeper than those of primary CRs beyond this energy. The latest observations by DAMPE further confirm an excess in the

secondary-to-primary flux ratio of CRs at high energies (Dampe Collaboration 2022).

To explain these observations, a spatially dependent CR propagation model has been developed. In contrast to conventional models that assume uniform propagation of CRs across the Galaxy, we propose the following: (1) CR propagation depends on the local distribution of matter (Guo & Yuan 2018; Guo et al. 2016; Evoli et al. 2012); (2) local CR sources act as both a potential well, confining local CRs, and a barrier, impeding external CRs from penetrating these regions (Yao et al. 2024; Nie et al. 2024; Tomassetti 2012); and (3) local CRs primarily consist of two components—component A, comprising CRs accelerated from distant sources and diffused into the region, which dominates at low energies, and component B, consisting of CRs from local sources, which dominate at high energies (Yao et al. 2024; Nie et al. 2024). High-energy phenomena in the Galactic vicinity are thus predominantly driven by local sources. This propagation model effectively accounts for the observed CR spectral features. However, observa-

Corresponding author: Yu-Hai Ge
geyh@ihep.ac.cn

Corresponding author: Yi-Qing Guo
guoyq@ihep.ac.cn

tions of diffuse gamma-ray emissions in the Galaxy and extended emissions from local CR sources may provide further validation of this propagation framework.

Gamma-ray extended emissions observed near pulsars confirm the existence of regions around them that exhibit slower diffusion relative to the interstellar medium (ISM). Since the morphology of pulsar halos follows the spatial distribution of their parent electrons/positrons, they serve as ideal probes for studying local CR propagation in the Galaxy. Observations of extended radiation from pulsars at different energy bands provide an opportunity to test our model. Recently, the Milagro Collaboration (Abdo et al. 2009), High-Altitude Water Cherenkov Observatory (HAWC) (Abeysekara et al. 2017), HESS (H. E. S. S. Collaboration et al. 2023), and Fermi-LAT (Di Mauro et al. 2019) have all revealed radiation from the Geminga halo. Notably, the Milagro Collaboration reported gamma-ray radiation from the Geminga direction extending over 2 degrees and spanning the energy range of 1-100 TeV. This observation was confirmed by HAWC, which detected extended gamma-ray emissions coincident with the position of Geminga. However, a decade-long analysis of Fermi-LAT data indicates no significant extended emission beyond the Geminga region in the 10-500 GeV energy range (Quattrocioni et al. 2019; Xi et al. 2019). Therefore, we believe that local CR halos play a crucial role in the propagation of CRs in the Galaxy, and investigating the mechanisms that generate the observability of pulsar extended emissions at different energy bands is essential.

This work focuses on the observations of radiation spectra from different energy bands in the Geminga halo, made by Fermi-LAT and HAWC, as well as the distribution of diffuse gamma rays near Geminga observed by LHAASO, and the measurement of cosmic-ray positrons by AMS-02. These observations constrain the injection and diffusion of cosmic-ray particles in the Geminga halo and allow us to investigate the observability of extended radiation from the Geminga halo across different energy ranges. We aim to test the proposed spatially dependent cosmic-ray propagation model. The structure of this paper is as follows: Section 2 introduces the diffusion of electrons/positrons in the pulsar halo; Section 3 discusses our results; and Section 4 provides a summary and outlook for future work.

2. DIFFUSION IN HALO

The local halo plays an essential role in the cosmic ray propagation process. The fluctuating structure observed in the radial distribution of diffuse gamma rays by LHAASO may be due to the contribution from lo-

cal sources that cannot be fully subtracted, particularly in the regions near the Geminga and Cygnus bubbles. Therefore, first, we use the spatially dependent propagation model proposed in previous work (see Appendix A) to simulate the distribution of Galactic background cosmic rays and the corresponding background diffuse gamma-ray radiation they produce. Then, we consider the halo as a slow diffusion region and, using the Geminga halo as an example, calculate its radiation spectrum to explain the latest observational data from LHAASO, Fermi-LAT, and HAWC. Finally, we discuss the observability of the Geminga halo signal under the contamination of the background radiation.

The diffusion coefficient around the pulsar, estimated from gamma-ray observations, suggests that it may be several hundred times smaller than the average value across the entire Milky Way. This slow diffusion could be caused by electrons/positrons escaping from the pulsar itself or by turbulent regions generated by cosmic ray particles escaping from the pulsar’s progenitor supernova remnant. Therefore, in our current work, we treat the diffusion of cosmic ray particles from the pulsar halo as a spherically symmetric “two-zone” diffusion model, which consists of slow diffusion within the halo and faster diffusion in the interstellar medium. The diffusion coefficient is mathematically described as (Jóhannesson et al. 2019):

$$D = \beta \left(\frac{\mathcal{R}}{\mathcal{R}_0} \right)^\delta \begin{cases} D_h, & r < r_i \\ D_h \left[\frac{D_0}{D_h} \right]^{\frac{r-r_i}{r_o-r_i}}, & r_i \leq r \leq r_o \\ D_0, & r > r_o, \end{cases} \quad (1)$$

where β represents the particle velocity in units of the speed of light, D_0 is the normalization of the diffusion coefficient in the general ISM, D_h is the normalization for the diffusion coefficient within the SDZ with radius r_i , \mathcal{R} is the particle rigidity, and \mathcal{R}_0 is the normalization (reference) rigidity. The zone between r_i and r_o is a transition layer where the normalization of the diffusion coefficient increases exponentially from D_h to the ISM value D_0 .

The electrons/positrons injected into the halo by the pulsar propagate through diffusion. A smooth power-law cutoff function describes the injection spectrum of the electrons/positrons.

$$\frac{d\rho}{dE} \propto E_k^{-\gamma_0} \left[1 + \left(\frac{E_k}{E_b} \right)^{\frac{\gamma_1-\gamma_0}{s}} \right]^{-s} \quad (2)$$

Here, E_b is break energy, γ_0 , and γ_1 are spectral indices for low and high energy bands, and s represents

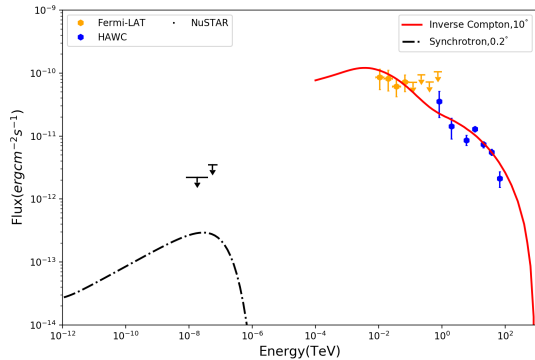


Figure 1. The multi-wavelength non-thermal emission from the Geminga pulsar halo as compared to the upper limits in the X-ray band obtained using XMM–Newton and NuSTAR data (Manconi et al. 2024) and Fermi-LAT (Di Mauro et al. 2019) and HAWC (Abeysekera et al. 2017) observations. The red line represents the angle-integrated inverse Compton radiative spectrum within 10° around the Geminga, and the black dot-dashed represents synchrotron emission within 0.2° .

the smoothness parameter. In this work, we fixed $E_b = 10\text{GeV}$, $\gamma_0 = 1.0$, and $s = 0.5$.

3. RESULTS

In this section, we present our computational results, which include the multi-band non-thermal radiation energy spectrum of the Geminga halo, the distribution of diffuse gamma rays in the Galactic disk, and the map distribution of signal intensities for the background and halo in the Geminga region. We also discuss the mechanisms that lead to these distributions and shapes forming near the pulsar. In calculating the background signals of the diffuse gamma rays from the Galactic disk, the Geminga halo, and the spectral components of the background radiation in the halo region, it is necessary to compute the distribution of cosmic ray particles in the Milky Way. We use the B/C and cosmic ray proton spectra observed near Earth to constrain the relevant parameters of the propagation model. Appendix A shows that we use a spatially dependent cosmic ray propagation model to accurately reproduce the observed B/C and proton spectra, with the values of the relevant parameters listed in Table 1.

3.1. Emissions from the Geminga pulsar halo

To reproduce the observed phenomena from the Geminga halo, we used the model constructed using the method described in Section 2 to calculate the radiation energy spectrum and its morphological distribution from the Geminga halo. Figure 1 presents the multi-wavelength non-thermal radiation from the Geminga

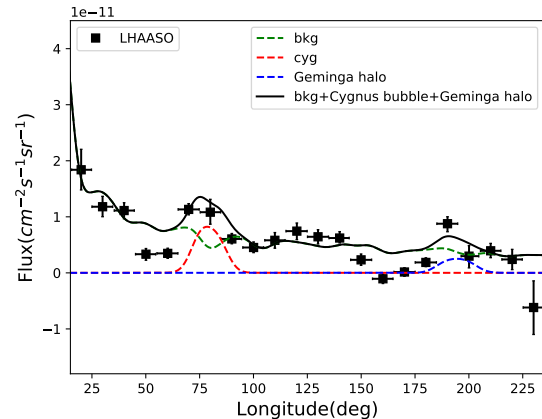


Figure 2. shows the flux of diffuse gamma-ray emissions in the Galactic longitude range of $|b| < 5^\circ$ with the energy range 10-63 TeV, in comparison with the LHAASO observations (Cao et al. 2023). The red dashed line represents the diffuse gamma components from the CR protons produced by the Cygnus bubble, the green dashed line represents the emission flux of diffuse gamma predicted by the CR SDP model, and the blue dashed line is components from the Geminga halo.

halo. Following the observational data, the synchrotron component is limited to the contribution within 0.2 degrees around the pulsar. In contrast, the high-energy IC component comes from the contribution of electron/positron pairs interacting with the cosmic background radiation via inverse Compton scattering in the 10° region. By using the upper limit data from the low-energy segment from NuSTAR and the observational data from Fermi-LAT and HAWC in the high-energy range, the magnetic field of the halo was determined to be $B_0 \sim 3\mu\text{G}$. The scale of the pulsar halo’s slow diffusion region is about 50 pc, with a diffusion coefficient $D_b = 6.6 \times 10^{25} \text{cm}^2 \text{s}^{-1}$. In Figure 2, we present the distribution of the diffuse gamma rays in the Galactic disk. To compare with the LHAASO observational data, we processed the model-calculated data like the LHAASO data: 1) smoothing the theoretical data and 2) subtracting the contributions from point sources and extended sources when calculating the background radiation. Therefore, in this work, the sources detected by KM2A and those observed by other experiments summarized in TeVCat were all subtracted during the calculation of the diffuse radiation, especially in the regions of the Cygnus bubble and Geminga. The region of the Cygnus bubble was masked within about 6° , while the region around Geminga had its contribution removed within an 8° radius, which is about 2.5 times larger than the masked regions of other sources listed in TeVCat. As shown in the Figure 2, even with the removal

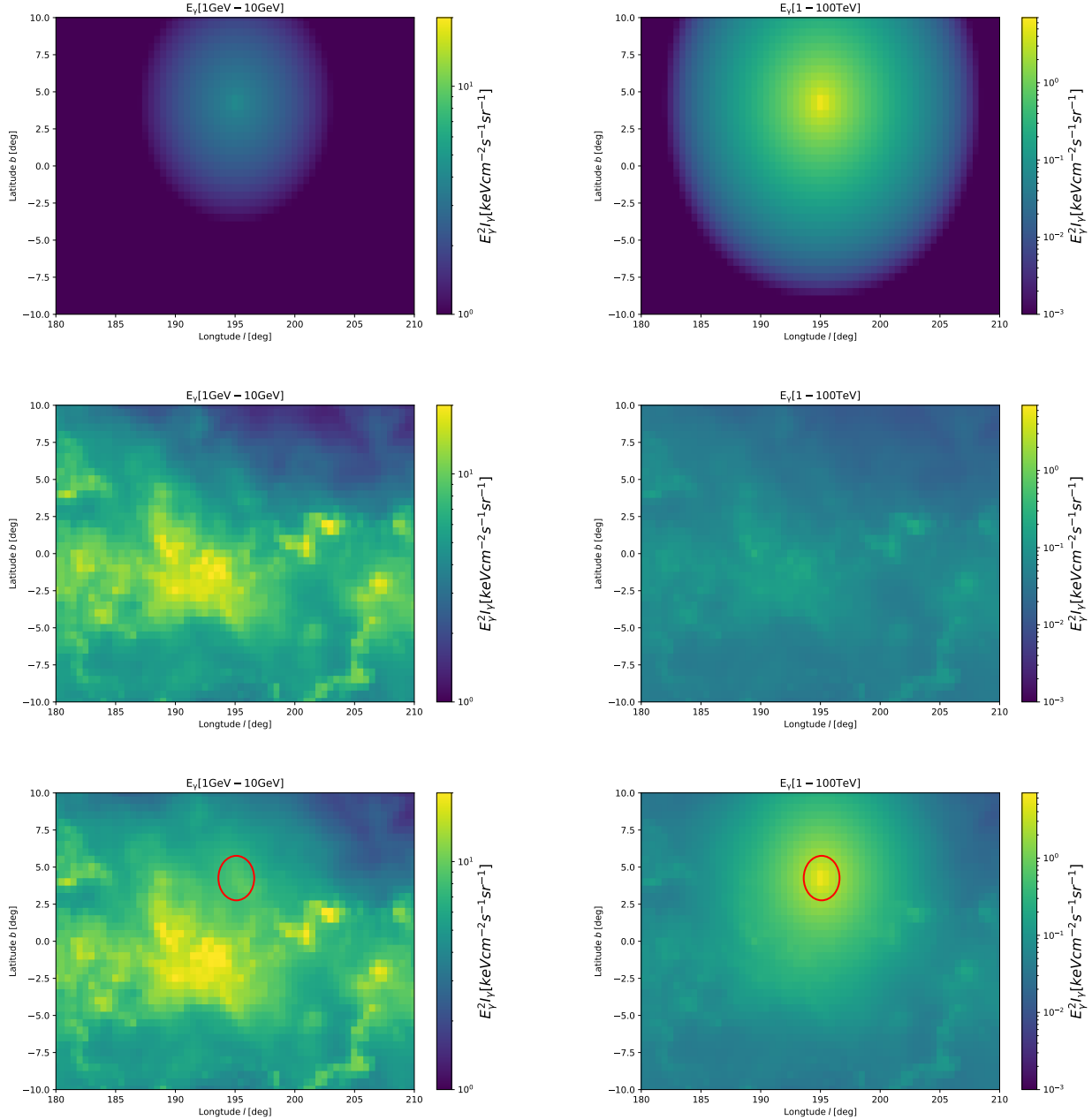


Figure 3. Gamma-ray flux maps (left panel), which include individual (up left panel: signal from Geminga pulsar halo, and left middle: background components) and Comprehensive (up left panel: total emission components) maps in the energy band 1–10 GeV. Right panel maps are the same as up panel but in the range 1–100 TeV.

of contributions from extended sources in a larger area, the Cygnus bubble and Geminga halo still provide dominant contributions. The detailed calculation process of the Cygnus bubble component in Figure 2 can be found in our previous work (Nie et al. 2024). Similar to the diffusion of electrons/positrons in the halo in this work, the Cygnus bubble is also considered a slow diffusion region, and its energy spectrum, morphological distribu-

tion, and the diffuse gamma-ray structure in the region have been well reproduced.

3.2. Map of Geminga halo

In the vicinity of the Geminga pulsar, no radiation morphology was observed in the GeV energy range, but there is an extended radiation in the TeV range. To investigate the mechanism behind this phenomenon, we used the observational data of the multi-wavelength en-

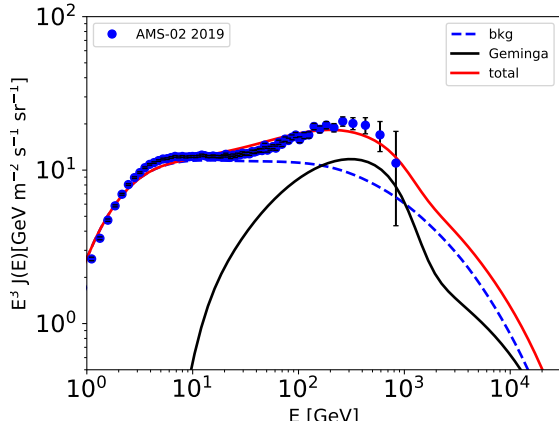


Figure 4. The predicted spectrum of positrons and observed data from AMS-02 (Aguilar et al. 2019).

ergy spectrum from the Geminga halo, as well as the model parameters derived from the constraints of the diffuse gamma-ray observations of the Galactic disk by LHAASO, to calculate the map signals of the Geminga halo and the background. As shown in Figure 3, in the 1-10 GeV energy range, the Geminga halo signal is relatively weak compared to the background intensity, to the point where the extended radiation morphology near the Geminga pulsar is almost invisible due to the contamination of the background. However, in the 1-100 TeV energy range, Geminga produces a signal much stronger than the background, and a significant radiation morphology remains even with the background contribution considered, consistent with the observations from Fermi and HAWC.

Theoretical models suggest that lower-energy electrons/positrons produce the GeV radiation through inverse Compton scattering with soft background photons. However, once the electrons/positrons escape from the pulsar, they propagate through the slow diffusion region near it and diffuse into the more distant and homogeneous normal Galactic environment. In the region where ($r < r_{in}$), the diffusion coefficient of particles is at least two orders of magnitude smaller than in other regions due to the spatial-dependence of D_h , meaning that the density of electrons/positrons that generate GeV radiation in this region is low. As a result, the GeV IC radiation flux decreases, and Fermi-LAT can almost not detect any radiation beyond the background.

On the other hand, for the parent electrons/positrons that generate TeV radiation, the larger diffusion coefficient allows them to have a larger effective diffusion radius, enabling them to escape from the slow diffusion region and generate radiation through inverse Compton scattering in a larger extended area. Therefore, there

is a strong extended source signal near the Geminga pulsar. This explains why the “bubble” structure remains in the diffuse gamma-ray distribution observed by LHAASO, even after subtracting the contribution from the 8° region around Geminga.

3.3. Contribution of the Geminga to the positron spectrum

The excess of cosmic ray positrons is observed in the experimental measurements of the cosmic ray positron flux in the energy range of 10 – 500 GeV (Aguilar et al. 2019, 2013; Adriani et al. 2009), which is higher than the expected flux according to the “standard cosmic ray propagation model”. However, our calculations show that while the spatial-dependent cosmic ray propagation model predicts a larger contribution at high energies (as illustrated by the blue dashed line in Figure 4), it still fails to match the observed experimental magnitude. Nevertheless, estimates based on electron energy losses suggest that sources on scales of \sim kpc might significantly contribute to the positrons observed on Earth (Aharonian et al. 1995).

Geminga is a middle-aged pulsar located about 250 pc from Earth, with an age of \sim 340 ky and a spin-down power of 3.2×10^{34} ergs $^{-1}$ (Faherty et al. 2007). Its distance and age provide strong grounds to believe it could be a major source of the positron excess. The spectrum of positrons obtained near Earth, as shown in Figure 4, is constrained by the data from Fermi, HAWC, and LHAASO. While the spectrum is nearly consistent with the observational data, it is difficult to distinguish between electrons and positrons in the halo, so Geminga may contribute less than 50% of the observed positrons. This suggests that other nearby candidate sources or alternative physical processes, such as dark matter annihilation or proton-proton (p-p) interactions of cosmic rays from nearby sources, could also play a significant role and should not be ignored.

4. CONCLUSION AND SUMMARY

This paper investigates the transport and radiation properties of electrons/positrons in the Geminga halo using observational data from LHAASO, Fermi, and HAWC, with the GALPROP package as the simulation tool. It expands on the role of pulsar halos in the cosmic ray propagation process, explores the spatial dependence of diffuse gamma radiation, and tests the spatially dependent cosmic ray propagation models.

We reproduce the non-thermal radiation energy spectrum from the Geminga halo, and the extended radiation maps in the 1-10 GeV and 1-100 TeV energy ranges. Our findings suggest that only a tiny fraction of the

low-energy electrons/positrons injected by the Geminga pulsar may escape from its surrounding slow diffusion region and produce radiation in the extended area. The high-energy radiation phenomena near the pulsar (including the extended radiation observed by HAWC, which spans more than 2.6 degrees, and the “bump” structure in the diffuse gamma-ray radiation distribution observed by LHAASO in the region of the pulsar’s silver disk) are primarily caused by the contribution of high-energy electrons/positrons that escape the slow diffusion region. Our calculation results strongly support the idea that local sources mainly contribute to high-energy cosmic ray phenomena. On the one hand, the local cosmic ray halo prevents the propagation of external cosmic rays, and on the other hand, it limits the escape of local cosmic rays. Furthermore, diffuse gamma-ray radiation in the Milky Way shows spatial dependence. We believe that LHAASO will be able to observe the extended radiation from the Geminga halo and other TeV halos in the future, and more precise observations will further validate our conclusions.

ACKNOWLEDGEMENTS

This work is supported by the National Natural Science Foundation of China (12275279,12375103).

Appendix A. SPATIALLY-DEPENDENT PROPAGATION MODEL

Cosmic rays are accelerated during the active evolution phases of cosmic ray sources (such as supernova remnants (Nie et al. 2023; Ackermann et al. 2013; Amato 2014), pulsar wind nebulae (Nie et al. 2022; Cao et al. 2021; Lhaaso Collaboration et al. 2021; Zhu et al. 2015), the galactic center (Abeysekara et al. 2021), binary star systems (Mirabel 2012) and so on) and injected into the interstellar medium, where they freely diffuse. The diffusion timescale can last up to approximately 10 million years (Garcia-Munoz et al. 1977). During this diffusion process, cosmic rays interact with the surrounding material, producing secondary cosmic ray particles. For example, the fragmentation and decay of heavy nuclei produce secondary cosmic ray particles, including light nuclei (Li, Be, B) and antiparticles (antiprotons and positrons). Additionally, cosmic ray electrons and positrons interact with the ambient magnetic field and background radiation throughout their journey, resulting in energy loss. The entire dynamical behavior of cosmic ray propagation can be described by the following diffusion equation (Strong et al. 2007; Evoli et al. 2017):

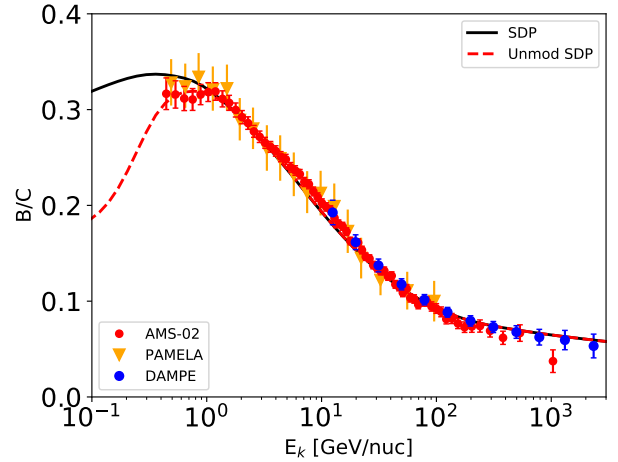


Figure 5. A comparison of the B/C ratio calculated using the CR SDP model with observational data from AMS-02 (Aguilar et al. 2017), PAMELA (Adriani et al. 2014), and DAMPE (Dampe Collaboration 2022) is presented. The red dashed line indicates the spectrum calculated without considering solar modulation. In this study, the solar modulation potential is consistently assumed to be 550 MeV.

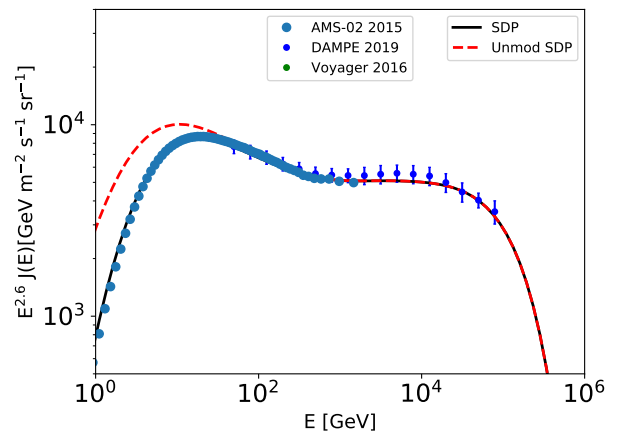


Figure 6. The CR proton spectrum is calculated using the CR SDP model and compared with observational data from AMS-02 (Aguilar et al. 2015) and DAMPE (An et al. 2019). The red dashed line shows the spectrum without including solar modulation effects.

Table 1. Parameters of the SDP model.

D_0 [$\text{cm}^2 \text{s}^{-1}$]	δ_0	N_m	ξ	n	v_A [km s^{-1}]	z_0 [kpc]
4.5×10^{28}	0.64	0.24	0.1	4.0	6	4.5

$$\begin{aligned} \frac{\partial \psi(\vec{r}, p, t)}{\partial t} = & Q(\vec{r}, p, t) + \vec{\nabla} \cdot (D_{xx} \vec{\nabla} \psi - \vec{V}_c \psi) \\ & + \frac{\partial}{\partial p} \left[p^2 D_{pp} \frac{\partial \psi}{\partial p} \right] \\ & - \frac{\partial}{\partial p} \left[\dot{p} \psi - \frac{p}{3} (\vec{\nabla} \cdot \vec{V}_c) \psi \right] - \frac{\psi}{\tau_f} - \frac{\psi}{\tau_r} \end{aligned} \quad (3)$$

where $\psi(\vec{r}, p, t)$ represents the CR density per unit of total particle momentum p at position \vec{r} , $Q(\vec{r}, p, t)$ describes the source term, D_{xx} denotes the spatial diffusion coefficient, \vec{V}_c is the convection velocity and τ_f and τ_r are the timescales for loss by fragmentation and radioactive decay, respectively. The CR diffusion depends on the distribution of CR sources $f(r, z)$, and the diffusion coefficient is described as (Guo et al. 2016; Guo & Yuan 2018)

$$D_{xx}(r, z, \mathcal{R}) = D_0 F(r, z) \beta^\eta \left(\frac{\mathcal{R}}{\mathcal{R}_0} \right)^{\delta_0 F(r, z)}, \quad (4)$$

where $\delta_0 F(r, z)$ describes the turbulent characteristics of the local medium environment and $D_0 F(r, z)$ represents the normalization factor of the diffusion coefficient at

the reference rigidity.

$$F(r, z) = \begin{cases} g(r, z) + [1 - g(r, z)] \left(\frac{z}{\xi z_0} \right)^n, & |z| \leq \xi z_0 \\ 1, & |z| > \xi z_0 \end{cases}, \quad (5)$$

here, ξz_0 denotes the half-thickness of the Galactic halo, and $g(r, z) = N_m / [1 + f(r, z)]$, where N_m is the normalization factor. The parameter n is used to describe the smoothness between the inner and outer halos, and the source distribution $f(r, z)$ is a cylindrically symmetric continuous distribution (Case & Bhattacharya 1996; Strong & Moskalenko 1998; Case & Bhattacharya 1998),

$$f(r, z) = \left(\frac{r}{r_\odot} \right)^{1.25} \exp \left[-\frac{3.87 (r - r_\odot)}{r_\odot} \right] \exp \left(-\frac{|z|}{z_s} \right), \quad (6)$$

Where $r_\odot = 8.5$ kpc and $z_s = 0.2$ kpc. The D_{pp} describes the re-acceleration process of particles during propagation, and its coupling relationship with the spatial diffusion coefficient D_{xx} is given by:

$$D_{pp} D_{xx} = \frac{4p^2 v_A^2}{3\delta(4 - \delta^2)(4 - \delta)} \quad (7)$$

where v_A is the Alfvén speed, and w is the ratio of magneto-hydrodynamic wave energy density to the magnetic field energy density, which can be fixed to 1.

REFERENCES

- Abdo, A. A., Allen, B. T., Aune, T., et al. 2009, *ApJ*, 700, L127, doi: [10.1088/0004-637X/700/2/L127](https://doi.org/10.1088/0004-637X/700/2/L127)
- Abeyssekara, A. U., Albert, A., Alfaro, R., et al. 2017, *Science*, 358, 911, doi: [10.1126/science.aan4880](https://doi.org/10.1126/science.aan4880)
- . 2021, *Nature Astronomy*, 5, 465, doi: [10.1038/s41550-021-01318-y](https://doi.org/10.1038/s41550-021-01318-y)
- Ackermann, M., Ajello, M., Allafort, A., et al. 2013, *Science*, 339, 807, doi: [10.1126/science.1231160](https://doi.org/10.1126/science.1231160)
- Adriani, O., Barbarino, G. C., Bazilevskaya, G. A., et al. 2009, *Nature*, 458, 607, doi: [10.1038/nature07942](https://doi.org/10.1038/nature07942)
- . 2014, *ApJ*, 791, 93, doi: [10.1088/0004-637X/791/2/93](https://doi.org/10.1088/0004-637X/791/2/93)
- Aguilar, M., Alberti, G., Alpat, B., et al. 2013, *Phys. Rev. Lett.*, 110, 141102, doi: [10.1103/PhysRevLett.110.141102](https://doi.org/10.1103/PhysRevLett.110.141102)
- Aguilar, M., Aisa, D., Alpat, B., et al. 2015, *Phys. Rev. Lett.*, 114, 171103, doi: [10.1103/PhysRevLett.114.171103](https://doi.org/10.1103/PhysRevLett.114.171103)
- Aguilar, M., Ali Cavasonza, L., Alpat, B., et al. 2017, *Phys. Rev. Lett.*, 119, 251101, doi: [10.1103/PhysRevLett.119.251101](https://doi.org/10.1103/PhysRevLett.119.251101)
- Aguilar, M., Ali Cavasonza, L., Ambrosi, G., et al. 2019, *Phys. Rev. Lett.*, 122, 041102, doi: [10.1103/PhysRevLett.122.041102](https://doi.org/10.1103/PhysRevLett.122.041102)
- . 2021, *Phys. Rep.*, 894, 1, doi: [10.1016/j.physrep.2020.09.003](https://doi.org/10.1016/j.physrep.2020.09.003)
- Aharonian, F. A., Atoyan, A. M., & Voelk, H. J. 1995, *A&A*, 294, L41
- Amato, E. 2014, *International Journal of Modern Physics D*, 23, 1430013, doi: [10.1142/S0218271814300134](https://doi.org/10.1142/S0218271814300134)
- An, Q., Asfandiyarov, R., Azzarello, P., et al. 2019, *Science Advances*, 5, eaax3793, doi: [10.1126/sciadv.aax3793](https://doi.org/10.1126/sciadv.aax3793)
- Atkin, E., Bulatov, V., Dorokhov, V., et al. 2018, *Soviet Journal of Experimental and Theoretical Physics Letters*, 108, 5, doi: [10.1134/S0021364018130015](https://doi.org/10.1134/S0021364018130015)
- Cao, Z., Aharonian, F. A., An, Q., et al. 2021, *Nature*, 594, 33, doi: [10.1038/s41586-021-03498-z](https://doi.org/10.1038/s41586-021-03498-z)
- Cao, Z., Aharonian, F., An, Q., et al. 2023, *Phys. Rev. Lett.*, 131, 151001, doi: [10.1103/PhysRevLett.131.151001](https://doi.org/10.1103/PhysRevLett.131.151001)
- Case, G., & Bhattacharya, D. 1996, *A&AS*, 120, 437

- Case, G. L., & Bhattacharya, D. 1998, *ApJ*, 504, 761, doi: [10.1086/306089](https://doi.org/10.1086/306089)
- Dampe Collaboration. 2022, *Science Bulletin*, 67, 2162, doi: [10.1016/j.scib.2022.10.002](https://doi.org/10.1016/j.scib.2022.10.002)
- Di Mauro, M., Manconi, S., & Donato, F. 2019, *Phys. Rev. D*, 100, 123015, doi: [10.1103/PhysRevD.100.123015](https://doi.org/10.1103/PhysRevD.100.123015)
- Evoli, C., Gaggero, D., Grasso, D., & Maccione, L. 2012, *Phys. Rev. Lett.*, 108, 211102, doi: [10.1103/PhysRevLett.108.211102](https://doi.org/10.1103/PhysRevLett.108.211102)
- Evoli, C., Gaggero, D., Vittino, A., et al. 2017, *J. Cosmology Astropart. Phys.*, 2017, 015, doi: [10.1088/1475-7516/2017/02/015](https://doi.org/10.1088/1475-7516/2017/02/015)
- Faherty, J., Walter, F. M., & Anderson, J. 2007, *Ap&SS*, 308, 225, doi: [10.1007/s10509-007-9368-0](https://doi.org/10.1007/s10509-007-9368-0)
- Garcia-Munoz, M., Mason, G. M., & Simpson, J. A. 1977, *ApJ*, 217, 859, doi: [10.1086/155632](https://doi.org/10.1086/155632)
- Guo, Y.-Q., Tian, Z., & Jin, C. 2016, *ApJ*, 819, 54, doi: [10.3847/0004-637X/819/1/54](https://doi.org/10.3847/0004-637X/819/1/54)
- Guo, Y.-Q., & Yuan, Q. 2018, *Phys. Rev. D*, 97, 063008, doi: [10.1103/PhysRevD.97.063008](https://doi.org/10.1103/PhysRevD.97.063008)
- H. E. S. S. Collaboration, Aharonian, F., Ait Benkhali, F., et al. 2023, *A&A*, 673, A148, doi: [10.1051/0004-6361/202245776](https://doi.org/10.1051/0004-6361/202245776)
- Jóhannesson, G., Porter, T. A., & Moskalenko, I. V. 2019, *ApJ*, 879, 91, doi: [10.3847/1538-4357/ab258e](https://doi.org/10.3847/1538-4357/ab258e)
- Lhaaso Collaboration, Cao, Z., Aharonian, F., et al. 2021, *Science*, 373, 425, doi: [10.1126/science.abg5137](https://doi.org/10.1126/science.abg5137)
- Manconi, S., Woo, J., Shang, R.-Y., et al. 2024, *A&A*, 689, A326, doi: [10.1051/0004-6361/202450242](https://doi.org/10.1051/0004-6361/202450242)
- Mirabel, I. F. 2012, *Science*, 335, 175, doi: [10.1126/science.1215895](https://doi.org/10.1126/science.1215895)
- Nie, L., Liu, Y., & Jiang, Z. 2023, *ApJ*, 952, 100, doi: [10.3847/1538-4357/acda29](https://doi.org/10.3847/1538-4357/acda29)
- Nie, L., Liu, Y., Jiang, Z., & Geng, X. 2022, *ApJ*, 924, 42, doi: [10.3847/1538-4357/ac348d](https://doi.org/10.3847/1538-4357/ac348d)
- Nie, L., Qian, X.-L., Guo, Y.-Q., & Liu, S.-M. 2024, *ApJ*, 974, 276, doi: [10.3847/1538-4357/ad7eab](https://doi.org/10.3847/1538-4357/ad7eab)
- Quattrocioni, V., Consolini, G., Marcucci, M. F., & Materassi, M. 2019, *ApJ*, 878, 124, doi: [10.3847/1538-4357/ab1e47](https://doi.org/10.3847/1538-4357/ab1e47)
- Strong, A. W., & Moskalenko, I. V. 1998, *ApJ*, 509, 212, doi: [10.1086/306470](https://doi.org/10.1086/306470)
- Strong, A. W., Moskalenko, I. V., & Ptuskin, V. S. 2007, *Annual Review of Nuclear and Particle Science*, 57, 285, doi: [10.1146/annurev.nucl.57.090506.123011](https://doi.org/10.1146/annurev.nucl.57.090506.123011)
- Tomassetti, N. 2012, *ApJ*, 752, L13, doi: [10.1088/2041-8205/752/1/L13](https://doi.org/10.1088/2041-8205/752/1/L13)
- Xi, S.-Q., Liu, R.-Y., Huang, Z.-Q., Fang, K., & Wang, X.-Y. 2019, *ApJ*, 878, 104, doi: [10.3847/1538-4357/ab20c9](https://doi.org/10.3847/1538-4357/ab20c9)
- Yao, Y.-H., Dong, X.-L., Guo, Y.-Q., & Yuan, Q. 2024, *Phys. Rev. D*, 109, 063001, doi: [10.1103/PhysRevD.109.063001](https://doi.org/10.1103/PhysRevD.109.063001)
- Zhu, B.-T., Fang, J., & Zhang, L. 2015, *MNRAS*, 451, 3145, doi: [10.1093/mnras/stv1140](https://doi.org/10.1093/mnras/stv1140)